Integrated modelling: coupling of surface evolution and plasma-impurity transport[☆]

K. Schmid[a,*], F. Effenberg[b], A. Dinklage[c], L. Rudischhauser[c], Y. Gao[c], M. Mayer[a], S. Brezinsek[d], J. Geiger[c], G. Fuchert[c], V. Miklos[e], H. Smith[c], Y. Turkin[c], K. Rahbarnia[c], T. Stange[c], K. Ipp[c], J. Brunner[c], U. Neuner[c], A. Pavone[c], U. Hoefel[c], H. Ipp[c], W7-X Team[c]

[a] *Max-Planck-Institut für Plasmaphysik, Boltzmannstraße 2, D-85748 Garching b. München Germany*
[b] *Princeton Univ, Princeton Plasma Phys Lab, POB 451, Princeton, NJ 08543 USA*
[c] *Max-Planck-Institut für Plasmaphysik, 17491 Greifswald, Germany*
[d] *Forschungszentrum Jülich GmbH, Jülich 52425, Germany*
[e] *Center for Energy Research, Budapest, Hungary*

Abstract

During the interaction of the scrape off layer (SOL) plasma with the first wall the evolution of both wall and plasma are tightly coupled: The erosion of the first wall leads to an impurity concentration in the plasma which affects the particle and power balance in the plasma. In turn the impurities, when leaving the plasma via transport, can form deposits and mixed materials, far away from their initial source location. These deposits can be eroded, allowing the impurities to stepwise migrate through the fusion device until they end up at a location where the plasma at the wall is cold enough and no further erosion occurs. To describe these processes an integrated model of surface evolution and plasma transport of impurities is needed. The WallDYN code achieves this required coupling of processes by parameterising the output of surface evolution- and plasma impurity-migration-codes by analytical models. For a given fixed background plasma it evolves the surface composition, derives impurity flux into and from the plasma and can from this derive the impurity densities in the plasma. This paper will show the importance of including this recycling of impurities at the wall in impurity migration modelling: The $^{13}CH_4$ seeding experiment performed in the Wendelstein 7-X Stellerator is modelled using the recent extension of the WallDYN code to 3D plasma and wall geometries. A comparison with post mortem analysis of the ^{13}C deposition shows both qualitative and quantitative agreement with the WallDYN calculations.

1. Introduction

During the interaction of the scrape off layer (SOL) plasma with the first wall the evolution of both the plasma and the wall are tightly coupled [1]: The wall material is eroded by physical or chemical erosion and enters the plasma as an impurity species leading to a certain impurity density n_Z in the plasma. These plasma impurities migrate and after a number of (re-) erosion/(re-) deposition steps they form layers at locations where their non-reflected influx Γ^{IN} exceeds their re-erosion flux Γ^{ERO}. These layers then act as new sources of impurities, which again undergo migration thus changing both n_Z in the plasma and their Γ^{IN} at the wall. The changes in Γ^{IN} result in variations of n_Z and of the layer growth rate. The changes in n_Z also affect the plasma parameters temperature T_e and density n_e via line radiation and also dilute the plasma. These changes in T_e and n_e in turn again affect Γ^{ERO} through changes in the incident particle energy and background main ion plasma flux.

Elaborate models have been developed to describe each of the processes separately: The SOL plasma with a fixed first wall composition is modelled in 2D by SOLPS [2] or 3D by EMC3-EIRENE [3]. The migration of impurities on

[☆] Oral MO06(B)

[*] K. Schmid
Email address: klaus.schmid@ipp.mpg.de (K. Schmid)

a fixed plasma background is modelled by e.g. DIVIMP [4] or ERO [5]. The surface evolution due to erosion deposition for a fixed incident particle spectrum is modelled by dynamic TRIM codes [6, 7] like SDTrim.SP. To describe the coupling and feedback between these processes one can parameterise the codes output and setup continuity equations to derive the time evolution of Γ^{IN}, Γ^{ERO} and n_Z as is in done in the WallDYN [8, 9] approach. This WallDYN approach requires simplified models, but allows for a computationally efficient, non-iterative solution of the coupled problem. The WallDYN approach has been successfully applied to JET-ILW [10] and ASDEX-Upgrade [11], showing that one of the key process in modelling Γ^{IN} and n_Z is to take the multiple re-erosion and re-deposition steps of the migrating impurity into account. This presentation will first describe the WallDYN approach of parameterisation of surface evolution and impurity migration in the plasma by analytical models which describe dynamic TRIM and trace impurity transport code output. Finally first modelling results of the $^{13}CH_4$ seeding experiment in Wendelstein 7-X (W7-X) with a carbon divertor, obtained with the recently developed extension of WallDYN to 3D geometries [12, 13], will be presented and compared to first post mortem analysis results of ^{13}C deposition.

2. The WallDYN approach

The WallDYN approach to integrated modelling of surface dynamics and impurity influxes from the plasma is based on parameterisations of plasma trace impurity migration models (e.g. DIVIMP [4]) and of surface dynamics models (e.g. SDTrim.SP [6]). It has been extensively described in [12, 8, 9, 14] therefore here only the parts pertaining to impurity recycling will be revisited briefly.

The total influx $\Gamma^{Source}_{ei,wk}$ into the plasma of element ei from wall wk is given by the sum of reflected, eroded (sublimated) and injected/seeded flux. $\Gamma^{Source}_{ei,wk}$ is an influx of neutral particles into the plasma which are eventually ionised and are transported by the plasma until they impact on another wall element wj at a charge state qi. This redistribution of the sources $\Gamma^{Source}_{ei,wk}$ is described by the migration matrix $m_{ei,wk,wj,qi}$. Thus the impurity influx of element ei at charge state qi $\Gamma^{In}_{ei,wj,qi}$ on wall element wj can be written as a matrix/vector product $\Gamma^{In}_{ei,wj,qi} = m_{ei,wk,wj,qi} \cdot \Gamma^{Source}_{ei,wk}$. So the total equation of impurity recycling can be written as in eq. 1

$$\begin{aligned}
\Gamma^{In}_{ei,wj,qi} &= \sum_{wk} m_{ei,wk,wj,qi} \left(\Gamma^{Ero}_{ei,wk} + \Gamma^{Refl}_{ei,wk} + \Gamma^{Seed}_{ei,wk}\right) \\
\Gamma^{Refl}_{ei,wk} &= \sum_{qi} (1 - R_{ei,wk,qi})\, \Gamma^{In}_{ei,wk,qi} \qquad (1) \\
\Gamma^{Ero}_{ei,wk} &= \sum_{em} \sum_{qm} \Gamma^{In}_{em,wk,qm}\, Y_{ei,em,wk,qm}
\end{aligned}$$

The reflection and erosion fluxes are determined by the respective erosion and reflection yields $R_{ei,wk,qi}$ and $Y_{ei,em,wk,qm}$. They both depend on the composition of the surface which in WallDYN is described by the areal density $\delta_{ei,wk}$ $\left(m^{-2}\right)$ of elements ei on wall wk. It is this dependence of the yields on $\delta_{ei,wk}$ that couples the impurity fluxes $\Gamma^{In}_{ei,wj,qi}$ from the plasma with the composition state of the surface described by $\delta_{ei,wk}$. The coupling of $\Gamma^{In}_{ei,wj,qi}$ and $\Gamma^{Ero}_{ei,wk}, \Gamma^{Refl}_{ei,wk}$ leads to a time evolution of $\delta_{ei,wk}$ which in turn leads to a time evolution of $\Gamma^{Source}_{ei,wk}$ and therefore also of $\Gamma^{In}_{ei,wj,qi}$. Thus to describe impurity recycling a surface model for the evolution of $\delta_{ei,wk}$ is needed. This surface erosion/mixing model is described in detail in [15] and is basically a flux balance between influxes and erosion/reflection fluxes from the surface plus an exchange flux with the bulk $\Gamma^{Bulk}_{ei,wk}$ that maintains the total areal density of all elements in a thin ($\approx 1nm$) surface layer, the reaction zone (RZ), where all the erosion and mixing happens homogeneously. The main equation of the surface model is given in eq. 2

$$\begin{aligned}
\frac{\partial \delta_{ei,wk}}{\partial dt} &= \sum_{qi} \Gamma^{In}_{ei,wj,qi} - \left(\Gamma^{Ero}_{ei,wk} + \Gamma^{Refl}_{ei,wk}\right) + \Gamma^{Bulk}_{ei,wk} \\
\Gamma^{Ero}_{ei,wk},\ \Gamma^{Refl}_{ei,wk} &\quad \text{Depend on } \delta_{ei,wk} \text{ through the} \qquad (2) \\
&\quad \text{respective sputter- and reflection yields}
\end{aligned}$$

These two core equations of WallDYN amount to a parameterisation of complex trace impurity transport codes (eq. 1) and surface dynamics codes (eq. 2). They form a differential algebraic equation (DAE) system that is solved in a time dependent manner yielding the coupled time evolution of the impurity fluxes from the plasma onto the wall and the evolution of the surface composition. Equation 1 shows the importance of surface processes compared to plasma processes when interpreting impurity migration experiments: The resulting impurity influx is a product of plasma transport (described by $m_{ei,wk,wj,qi}$) and surface processes (described by erosion/reflection/seeding in $\Gamma^{Source}_{ei,wk}$). This means that both surface and plasma processes are of equal importance, one cannot interpret deposition patterns or measured plasma densities ($\propto \Gamma^{Source}_{ei,wk}$) without correctly describing both surface evolution and impurity transport in the plasma.

Approximating the trace impurity migration by a simple matrix/vector product in the context of WallDYN is possible if one assumes that the plasma transport times are much faster ($\approx$ ms) than the time scale the surface evolves on ($\approx$ s). Beyond that the matrix description of transport is an accurate representation of the output of an impurity migration code if trace approximation is assumed. The approximations that go into the surface model eq. 2 are more severe when compared to a code like SDTrim.SP [6]. In particular using only a single layer where all erosion and mixing takes place cannot describe any ion range profile driven effects. However at the low energies O(100eV) of impurities from the edge plasma, the ion range is short and thus range profile effects can be neglected. Still a direct comparison of eq. 2 with a comparable SDTrim.SP calculation needs to be done to test the applicability of the surface model for a particular application.

2.1. WallDYN surface model vs. SDTrim.SP

For modelling the $^{13}CH_4$ seeding experiment the surface model needs to describe the deposition of C isotopes on the C divertor plates and their (re-)erosion by H- and C-self-ions. To test the surface model, SDTrim.SP parameter scans were performed that simulate the impact of a mixture of H and ^{13}C on a ^{12}C surface. In these parameter scans the ^{13}C flux fraction (0 to 10%), the H-ion energy (50 to 150 (eV)) and the ^{13}C energy (100 to 300 (eV)) were varied. The SDTrim.SP calculations were performed in "dynamic" mode such that SDTrim.SP dynamically updates the composition of the target according to erosion, implantation and beam mixing effects. This dynamic mode is described in [7] and has been used before to interpret ion-beam deposition experiments [16]. From each calculation in the parameter scan the evolution of the surface composition averaged over a depth of 1 (nm), which matches the thickness of the RZ in WallDYN, was determined. The same parameter scan was also performed using the WallDYN surface model eq. 2. The required composition and energy dependent sputter- (C by H and C) and reflection- (C from C surfaces) yields were taken from static (fixed, non evolving surface composition) SDTrim.SP calculations. In the parameter scans only physical sputtering of C by C and C by H was included, later in the WallDYN calculations for W7-X, chemical erosion is also included. Also in contrast to the experiment only ^{13}C was included as incident species whereas in the W7X the incident flux contains both ^{13}C and ^{12}C. This simplification was introduced since the C-sputter yields by and reflection yields from ^{13}C and ^{12}C are essentially the same. Thus while an additional influx of ^{12}C would change the composition of a growing layer it would add no new physical processes to the code comparison.

In both kinds of calculations the evolution of the surface composition during exposure of an initially pure ^{12}C to a total (^{13}C + H) of flux $10^{20}(m^{-2}s^{-1})$ for 500 seconds was simulated. As an example, Fig. 1 shows the final concentration of ^{13}C as function of the H impact energy and ^{13}C influx fraction, for a ^{13}C impact energy of 100eV. This particular dataset with a ^{13}C impact energy of 100eV

was chosen since it contains the transition from net erosion (no ^{13}C accumulation at all) to net deposition (growth of a ^{13}C layer). Despite its simplicity, the WallDYN surface model reproduces the erosion/deposition transition well. The contour plots in Fig. 1 are meant to show the qualitative agreement for a particular subset of the parameter scan. A more quantitative comparison at each combination of parameters in the parameter scan yields a mean deviation of 11% +/- 1% for the ^{13}C concentration in equilibrium. This quantitative discrepancy is well below the uncertainties in the sputter and reflection yields themselves due to surface roughness effects (see e.g. [17]).

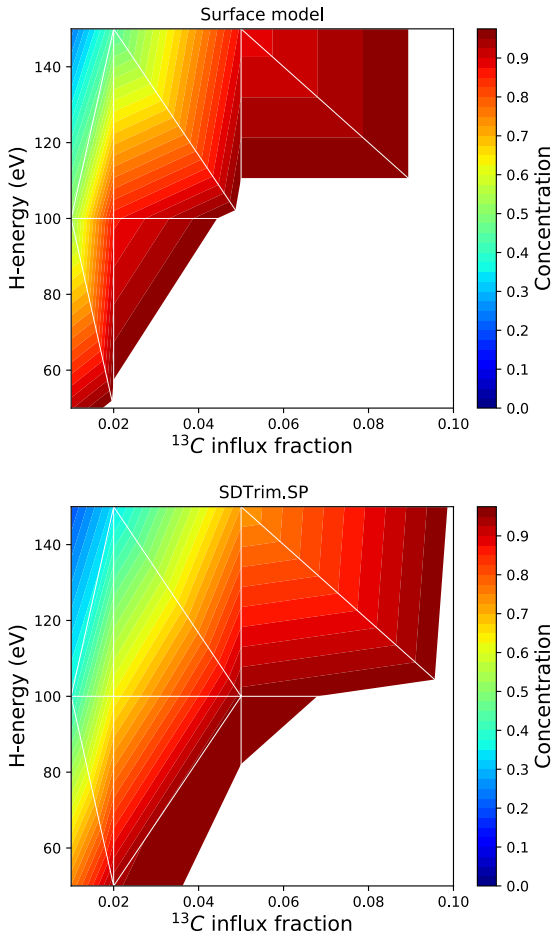

Figure 1: Comparison of the ^{13}C surface concentration calculated by the WallDYN surface model (top-figure) and by SDTrim.SP in dynamic mode (bottom-figure). The white areas are where the concentration of ^{13}C= 1 i.e. where continuous growth of a ^{13}C layer occurs

3. $^{13}CH_4$ seeding experiment in W7-X

The Wendelstein 7-X (W7-X) experiment [18] is a superconducting stellerator with a magnetic field of 2.5T and 30 m^3 plasma volume that can be heated with up to 10.5MW (7.5MeV ECRH and 3MW NBI). During the second operational phase (OP1.2) the plasma loaded components consisted of adiabatically loaded test divertor units (TDUs) with fine grain graphite panels. The rest of the wall is made of stainless steel. W7-X has a five fold toroidal symmetry and the TDUs are thus numbered 1 to 5 each with a lower (numbered 0) and an upper half module(numbered 1).

During the last 30 shots during OP1.2 a $^{13}CH_4$ puffing experiment was performed in a H-plasma to investigate the transport of C in and all C device. After the end of OP1.2 the TDU panels were removed to replace them with actively cooled components for long pulse operation. Analysing the ^{13}C deposits on the entire TDU offers a unique possibility to measure the global deposition patterns of C migrating through W7-X. During the 30 Shots numbered 20181018.11 to 20181018.40 a total of 4×10^{22} ^{13}C was injected in the form of $^{13}CH_4$ at a rate of 10^{20} (s^{-1}) through two valves from the He-beam diagnostic in the lower horizontal target of TDU module 30. The plasma was in attached state and thus the $^{13}CH_4$ were seeded directly into the scrape-off layer. All the shots were nominally identical with a core temperature and density of 2.8 to 3.2 (keV) and 5.6 to 6.0 10^{19} (m^{-3}) respectively. The plasmas were heated by 3.4 to 3.9MW ECRH only (NBI blips where applied for charge exchange spectroscopy only) and had radiated power fractions of 0.25 to 0.6, rising during the discharge due to seeding. The standard magnetic divertor configuration with 5 magnetic islands (edge transformation iota 5/5) was used. A summary plot of the time evolution of these discharge parameters is shown in Fig. 2 for shot 20181018.20 from the middle of the 30 seeding discharges.

For plasma wall interaction the edge conditions are of

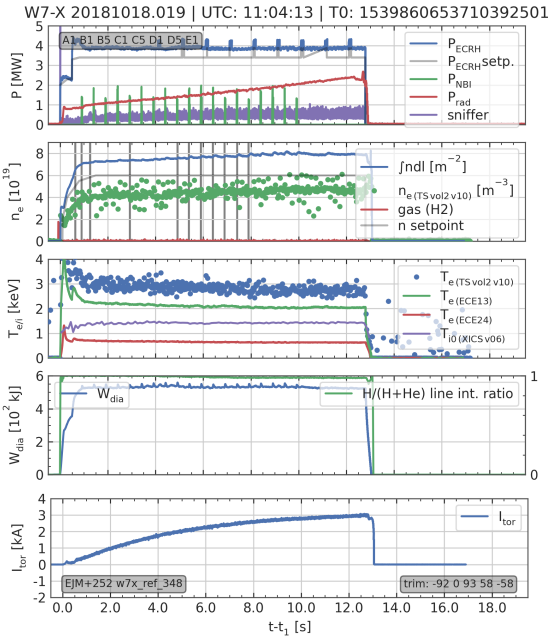

Figure 2: Overview plot of the global plasma parameters of a typical shot during the seeding experiment

more importance than the overview parameters in Fig. 2. The plasma edge was diagnosed by Langmuir Probes and partially also by Thomson scattering and the results are presented in section 4.2 During the seeding experiment spectroscopy was used to monitor the C and O impurities in the plasma. After removing the TDU components they were analysed using various techniques. Here we will focus the ion beam analysis of ^{13}C deposits from selected samples from TDU 30 [19].

4. Modelling the $^{13}CH_4$ seeding experiment in W7-X

The goal in modelling the $^{13}CH_4$ seeding experiment is to understand the mechanisms leading to the ^{13}C deposition patterns that were measured by post mortem analysis and to thus benchmark the applied modelling tools (EMC3-Eirene & WallDYN) such that predictions for future long pulse operation can be made. An overview of the modelling geometry can be seen in Fig. 3. It shows the upper and lower TDU halfs. In the lower half the horizontal and vertical target are separated by a pumping gap which is used as reference for poloidal distance measures in some of the plots.

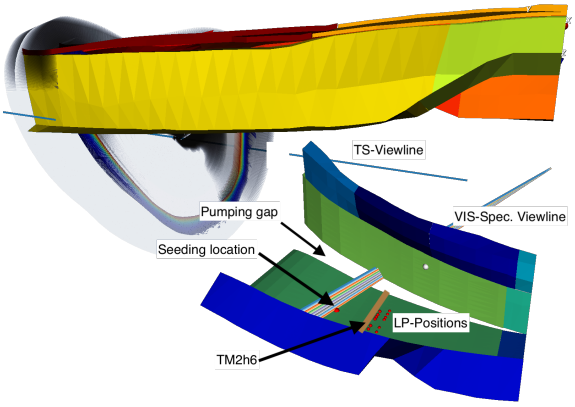

Figure 3: Overview of the modelling geometry: The Thomson Spectroscopy (TS) viewline together with the part of the computational grid that it intersects. Location of the $^{13}CH_4$ seeding valve and of the Langmuirprobes.

4.1. Modelling assumptions and limitations

The kinetic trace impurity transport module that was recently implemented in EMC3-Eirene [12, 13] can only treat atomic species i.e. no molecules like $^{13}CH_4$. Therefor the $^{13}CH_4$ seeding is modelled as injection of neutral ^{13}C thus neglecting the breakup chain of the molecule prior to ionisation of the ^{13}C atom. This amounts to assuming that the distance to ionisation O(cm) is small compared to the length O(m) traveled through the plasma as an ion prior to deposition on the wall. Computing the cumulative distribution of the lengths of the trajectories recorded during the migration simulations yields: 16% travel less than ≈ 0.1 (m) or more than ≈ 10 (m) and the median lies at ≈ 1 (m). This suggests that the above approximation is justified when investigating global migration patterns where 84% of the particles travel more than ≈ 0.1 (m). Spectroscopic measurements show that apart from C also O is present in the plasma. Since C is eroded very efficiently by O ions (see also section 4.3), O is added as background species that erodes C but does not deposit

on the surface. In the surface model only ^{13}C and ^{12}C make up the composition of the reaction zone and they are eroded by H-ions, H charge exchange neutrals (H-CX), O-ions and C-self-ions. For erosion by H and O chemical erosion is taken into account in addition to physical sputtering. However similar to the seeded $^{13}CH_4$ the chemical erosion products (CH_4, CO and CO_2) are treated a C atoms during re-distribution by the $m_{ei,wk,wj,qi}$ matrix.

WallDYN requires a charge state resolved incident flux $\Gamma^{In}_{ei,wj,qi}$ to compute erosion. For C isotopes this is calculated self consistently from the surface (re-)erosion & reflection rates in $\Gamma^{Source}_{C,wk}$ and the re-distribution matrix $m_{C,wk,wj,qi}$. For the background O fluxes a different approach is used since O is not assumed to accumulate in the surface thus a $\Gamma^{Source}_{O,wk}$ cannot be derived from erosion & reflection. Therefore to obtain a reasonable estimate of the background O influx at each charge state it is assumed that O, in equilibrium, recycles at 100% so all impacting O is re-emitted into the plasma (i.e. Γ^{In} becomes Γ^{Source}). To find the equilibrium $\Gamma^{In}_{O,wj,qi}$ for O an iterative approach is used: Initially a certain O flux ($m^{-2}s^{-1}$) is homogeneously emitted from all wall elements and is re-distributed by $m_{O,wk,wj,qi}$ yielding the influx of O onto each wall element after iteration 1 ($\equiv \Gamma^{In,1}_{O,wj,qi}$). Then, assuming 100% recycling, this influx $\Gamma^{In,1}_{O,wj,qi}$ is re-emitted from the wall elements and is then again re-distributed by $m_{O,wk,wj,qi}$ yielding $\Gamma^{In,2}_{O,wj,qi}$, the influx at iteration 2. This processes is continued until in equilibrium $\Gamma^{In,equil}_{O,wj,qi}$ is reached which takes $\approx$ 10 iterations. This $\Gamma^{In,equil}_{O,wj,qi}$ is then used as constant flux spectrum for O (similar to H-ions from the background plasma). The total O influx integrated over the surface area of 10^{19} O s^{-1} was chosen such that the Z_{eff} resulting from O and C in the plasma matches the experimental value of $\approx$ 1.3 along the Thomson-Spectroscopy view-line (see section 4.2). In the scrape off layer this corresponds to an average O plasma concentration of 0.1 to 0.5%.

The W7-X stellerator has a five fold symmetry i.e. each of the 5 TDU sectors are assumed to have the same plasma parameters. In addition inside each of the 5 sectors the plasma is up/down symmetric, meaning the second half of the sector is a copy of the first half mirrored across a plane normal to the Z-axis. Exploiting both the five fold- and the up/down- symmetry reduces the EMC3-Eirene simulation volume to $1/5 \times 1/2 = 1/10$th of the toroidal circumference. This reduction reduces the computational effort required both for the background plasma solution but also for the WallDYN calculation since 1/10th of the circumference also means only 1/10 of the wall surface areas N_{Wall} need to be treated. Due to its DAE nature, solving the equations requires inverting the system jacobi matrix whose size scales ${N_{Wall}}^2$. Therefore currently the maximum number of wall elements that can be handled by WallDYN is limited to $\approx$ 1000 and the W7-X simulations presented here use 880 wall elements which is close to this maximum. In general, exploiting this symmetry does not affect the level of approximation of the experiment, since the erosion/deposition/migration processes are the same in all of the 10 simulation volumes. However the single $^{13}CH_4$ seeding source, located in only one of the five sectors, breaks this symmetry and how well the current simulation symmetry assumptions approximate this, needs further thought: Simulating only volume number 1 of the 10 volumes of the circumference, overestimates the amount of ^{13}C that ends up on the walls, since some of the seeded ^{13}C could cross the boundaries of volume number 1 and end up in any of the other 9 volumes. Also some of the ^{13}C thus deposited away from volume number 1 might make it back into volume number 1 during the re-erosion/re-deposition chain. While this latter process of transport back to volume number 1 cannot be handled without a full 360° simulation, at least the loss from volume number 1 into the other volumes can be estimated: During the calculation of $m_{ei,wk,wj,qi}$ a single trace impurity transport calculation is performed for each wall element where element ei is launched from source wall element wk and the

deposition at each destination wall element wj at charge state qi is recorded. During these calculations also the trajectories in R, Z, Φ coordinates are recorded for a random sub-set of the traced particles. During the transport calculations these particle trajectories are projected back into simulation volume number 1 every time a particle crosses the boundaries. After the calculation these boundary projections can be easily detected since they involve a sign change in the Z-coordinate due to the up/down nature of symmetry. This allows to undo the boundary jumps and reconstruct the full 360° trajectories. In particular the actual toroidal angle Φ at the end of the trajectory can be computed which allows to determine in which of the 10 simulation volumes the particle would have ended up in a full 360° simulation. Fig. 4 shows a histogram of the final simulation volume from all particle trajectories that were recording during the computation of $m_{C,wk,wj,qi}$. Roughly 50% of re-distributed C launched in simulation volume 1 end up in there. This means that by scaling $m_{^{13}C,wk,wj,qi}$ by a factor of 0.5 should mimic the losses of ^{13}C to other simulation volumes. However as stated above this is a lower limit for the total seeded amount that ends up in simulation volume 1 since re-erosion of ^{13}C in any of the other simulation volumes might bring some more ^{13}C back.

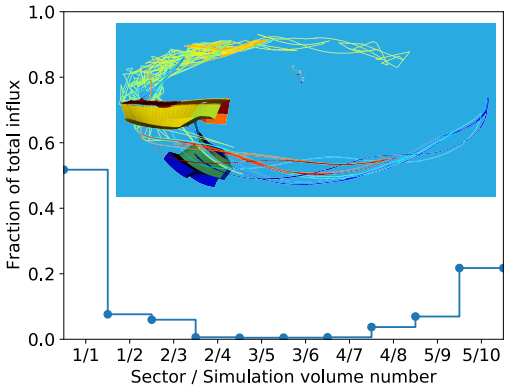

Figure 4: Fraction of C ending up at different sectors/simulation volumes when the boundary symmetry jumps are omitted in the traced C-impurity trajectories. The insert shows a reconstructed ^{13}C trajectory, without boundary condition projections back to simulation volume 1, whose extents are indicated by its upper and low TDU target elements

4.2. W7-X plasma solution

The kinetic trace impurity transport module [12] in EMC3 needs a background plasma solution (density n_e, temperatures T_e, T_i and flow pattern M) to compute the forces acting on an impurity from which its parallel motion along field lines is calculated. This plasma solution is determined by EMC3-Eirene which solves the reduced Braginskii fluid equations and uses Eirene to solve the kinetic transport equations for neutrals and molecules that recycle from the wall [3, 20, 21].

The $^{13}CH_4$ seeding experiment was performed in standard magnetic divertor configuration with 5 magnetic islands. The plasma was heated by 4MW ECRH. The upstream density was set to a fixed value of $2 \times 10^{19}\,(m^{-3})$ in the simulation. The parallel heat conductivity of electrons and ions was assumed to be classical whereas the perpendicular transport parameters for heat ($\chi_{\perp e,i} = 1.0\,(m^2 s^{-1})$) and particles ($D_\perp = 1.0\,(m^2 s^{-1})$) were assumed to be anomalous and are treated as free model parameters. For the background plasma solution the standard fluid impurity transport model and not the new kinetic trace impurity transport module was used. The reason is that the new kinetic transport module was specifically designed for use in WallDYN and terminates particles on first wall impact as is needed for calculating $m_{ei,wk,wj,qi}$ instead of recycling them (impurity recycling is handled later in WallDYN). In the standard fluid impurity model the impurities are launched proportionally to the local main ion wall flux with the proportionality constant set such that a certain total impurity influx (s^{-1}) is achieved. This total impurity influx is a free model parameter that is used to fit the experimentally observed radiative fraction.

To test the applicability of the plasma solution for later trace impurity calculations it was compared to available experimental data from Langmuir Probes (LP) [22] and

Thomson Scattering (TS) [23]. The LPs in the horizontal divertor target are used for comparison with EMC3-Eirene calculations. The n_e and T_e data from four (20181018.012, .020, .031, .040) of the 30 discharges of the seeding experiment were used for the comparison. For each discharge and each of the 10-LPs the cumulative distribution function (CDF) of n_e and T_e values in the time window from 4 to 12 sec. (since start of the ECRH) were determined. During this analysis n_e and T_e results with excessively large error bars ($\gg 100\%$) were omitted since this indicated that the LP model fitting had failed. From these CDFs the three n_e and T_e values corresponding to 16% ($\equiv$ lower), 50 % ($\equiv$ median), 84 % ($\equiv$ upper) of the CDF were determined to obtain parameter ranges for each LP. In Fig. 5 a comparison of the LP data with the EMC3-Eirene data is shown. The T_e data from EMC3-Eirene in

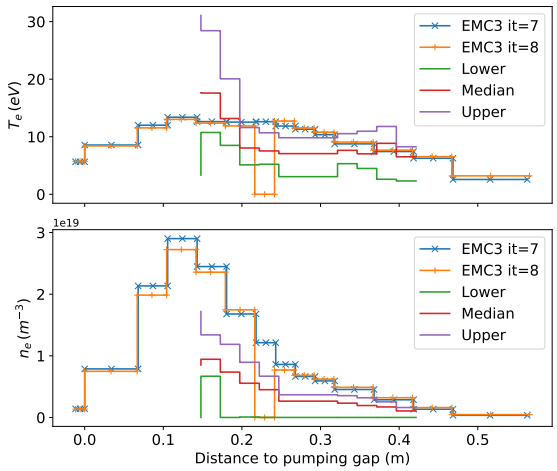

Figure 5: Comparison of Langmuir probe data experimental data from discharges 20181018.012, .020, .031, .040 with the EMC3-Eirene background plasma result

Fig. 5 compares reasonably well to the experimental T_e data from the LPs given the large variations in T_e during the different discharges. The comparison of the n_e data from EMC3-Eirene in Fig. 5 however shows that the EMC3-Eirene solution slightly overestimates n_e.

A comparison of the EMC3-Eirene plasma solution to upstream data from the TS diagnostic is shown in Fig. 6 for two discharges (20181018.012 and .040) from the seeding experiment. The data is plotted vs. r_{eff} which is the radius of a circle of the same area as the cross section of the flux surface the datapoint resides in. The T_e data from EMC3-Eirene matches the TS data quite well whereas the n_e is slightly too low. While the 30 consecu-

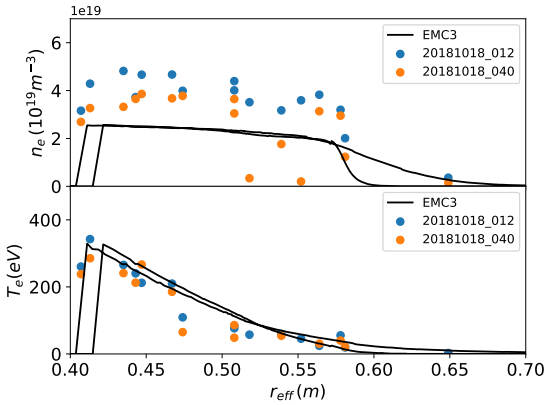

Figure 6: Comparison of n_e and T_e values from Thomson Scattering data with the EMC3-Eirene background plasma result

tive discharges of the $^{13}CH_4$ seeding experiment were all meant to be identical some scatter (see also variations in core n_e, T_e described in section 3) in the plasma parameters was present. Given this scatter the current state of the EMC3-Eirene background plasma is an acceptable representation of the experimental conditions and can be used for trace impurity transport modelling to interpret the ^{13}C migration patterns.

4.3. Surface process data

The WallDYN surface model requires numerous input parameters for each eroding/depositing element ei on each wall element wk to correctly compute (re-)erosion, reflection and deposition. The constant background flux of H-ions ($m^{-2}s^{-1}$) is taken from the post-processing routines in EMC3-Eirene. The constant background H-CX fluxes and energies are determined during the EMC3-Eirene neutral iteration (part of the EMC-Eirene solution process) where for each impact of a H-CX atom its impact location, particle monte-carlo weight and energy are recorded. The particle monte-carlo weight is converted to a H-CX

atom flux ($m^{-2}s^{-1}$) onto the wall element wk it impacted on, by scaling it with total recycling flux (s^{-1}) and dividing it by the area of the wall element wk. The also present constant background O ion fluxes are determined as explained in section 4.1. For charged impact species (H-ion and O-ions) the impact energy E for charge state q is derived from the standard sheath model expression (see e.g. [24]):

$$E(q) = 3\,q\,T_e + 2T_i \tag{3}$$

The T_e and T_i data at each wall element are also taken from the post-processing routines in EMC3-Eirene.

The chemical erosion of C by H ions and H-CX atoms depends on the surface temperature which is taken from IR-measurements performed during the seeding experiments. IR measurements are available for sectors 1, 2 & 3. The temperatures from the different sectors vary slightly due to small differences in the alignment between plasma and wall geometry. The temperature at the strike lines, where the highest power and particle fluxes occur, is in the range from 500 to 700K and there exist some hot-spots where the temperature even exceeds 800K. Finally for the WallDYN calculations of the ^{13}C deposition the temperature data from sector 3 was used from where the seeding took place. The chemical erosion yield of C by H depends on surface temperature, H impact energy and H influx. The model by Roth et al [25] was used to calculate the chemical erosion yield for each wall element. The same chemical yield was used for ^{13}C and ^{12}C. For the H and H-CX fluxes present in W7-X the flux dependence of chemical erosion shifts the maximum of the temperature dependence of the chemical yield to such high temperatures that the chemical yield in this simulation was essentially temperature independent and in the range 0.5 to 1.0%. Therefore the choice of using the wall temperature data from sector 3 has no significant impact on the simulation result. In addition to the chemical erosion C is also eroded by H via physical sputtering. The physical sputtering yield was calculated as function of energy and angle using SDTrim.SP and is added to the chemical yield.

The dependence of erosion of C by O ions as function of temperature and particle energy was extensively studied in [26, 27]. The erosion yield is essentially independent of temperature but has a significant energy dependence. The measurements in [26, 27] were performed at perpendicular angles of incidence. In order to derive yields for the oblique impact angles from the W7-X-plasma, a model was derived to describe the angle α and energy E dependence of C erosion by O. The model assumes that the erosion yield can be written as in eq. 4

$$\begin{aligned} Y^{O\to C}(E,\alpha) &= Y_{Chem}(E) + Y_{Phys}(E,\alpha) \qquad (4)\\ Y_{Chem}(E) &= \text{Energy dependent chemical yield}\\ Y_{Phys}(E,\alpha) &= \text{Energy and angle dependent physical sputtering yield} \end{aligned}$$

To derive $Y_{Chem}(E)$ the expected physical sputtering yield $Y_{Phys}(E, 0°)$ as computed by SDTrim.SP is subtracted from the experimental data $Y^{O\to C}(E, 0)$ in [27] leaving $Y_{Chem}(E)$ as a remainder. To obtain the erosion yield for a given impact angle α the physical sputtering contribution has to be added to $Y_{Chem}(E)$ to finally obtain the required $Y^{O\to C}(E, \alpha)$. In Fig. 7 the erosion yields of C by O is shown with the different contributions. At the oblique angle of impact (see also below) the yield quickly becomes > 1 thus even low fluxes of O can have a significant impact on C erosion even at low fractions of O in the incident flux.

To chose the impact angle of the eroding charged particles their trajectories along field lines and the ExB motion in the sheath potential prior to impact on the surface has to be included. According to [28] for a large range of plasma parameters and oblique angles between surface and magnetic field the impact angle is ≈60° with respect to the surface normal. However this is only true for perfectly flat surfaces, for rough surfaces the angles become less oblique and therefore an impact angle of 40° was chosen here. In Fig. 8 the erosion of C by H-species at each wall ele-

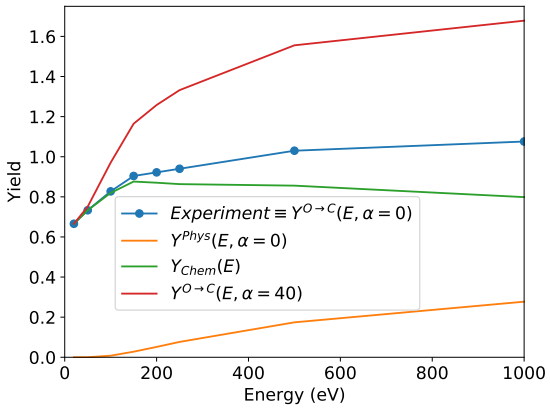

Figure 7: The different contributions to the C erosion yield by O model described in the text. Also shown the experimental data from [27]

ment is plotted versus impact energy at the wall location. At low energies the erosion by H is dominated by chemical erosion whereas at higher energies physical sputtering dominates. The distribution of erosion yields on the wall elements shows that chemical erosion of C by H dominates since the impact energy on most wall elements is < 100eV. The spikes in the "chemical + physical erosion" graphs are due to increased chemical erosion at hot-spots in the wall temperature data.

To compute the actual erosion flux of C from a wall element given the total erosion yield by a projectile element ej the composition dependence of the erosion has to be taken into account. For the mixtures of C isotopes in W7-X no significant preferential sputtering of either isotope is to be expected, therefore a linear dependence on the surface concentration $C_{ei,wk}$ in the RZ is assumed as in eq. 5.

$$\Gamma^{Ero}_{ei,wk} = \sum_{ej}^{Proj.} \sum_{qj}^{Chrg.} \left(\Gamma^{In}_{ej,wk,qj}\ Y\left(E(qj),\alpha\right)\ C_{ei,wk}\right) \quad (5)$$

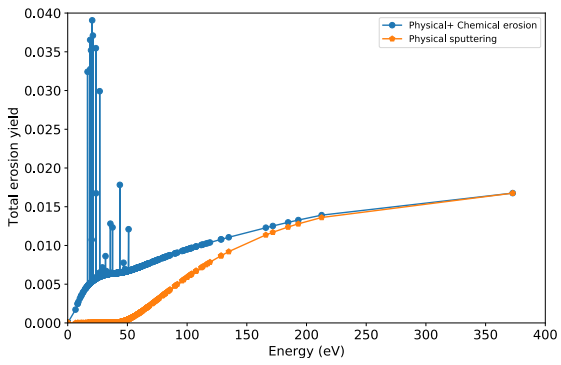

Figure 8: The total (Chem. + Phys.) and physical erosion yield for H on C for all wall elements in the WallDYN simulation sorted by impact energy.

5. Results

In Fig. 9 an overview plot of the the total deposited amount of ^{13}C in units of $(10^{20}m^{-2})$ after seeding for 400 seconds at 10^{20} ^{13}C (s^{-1}) is shown. For this calculation the redistribution matrix was not scaled by 50% and this result is an upper limit for the deposited amount as discussed in section 4.1. The ^{13}C deposition in Fig. 9 shows strong

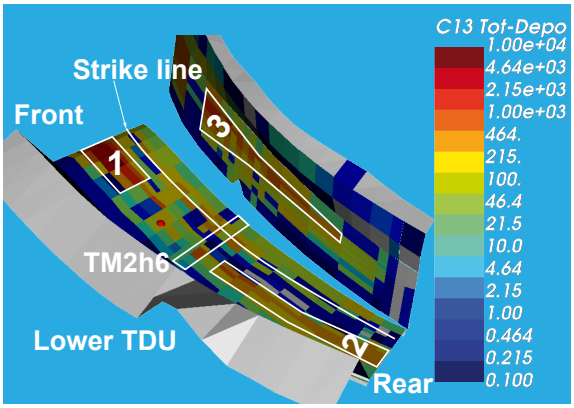

Figure 9: The total deposited amount of ^{13}C $(10^{20}m^{-2})$ during the seeding experiment as calculated by WallDYN. Three deposition regions are numbered and the location of post mortem analysis is marked

toroidal and poloidal variations. Qualitatively, three main deposition regions are numbered in Fig. 9. The color scale is logarithmic and the total deposited values range mainly from 10^2 to $10^4(10^{20}m^{-2})$. The ^{13}C is seeded directly into one of the magnetic islands from where the background plasma streams in both directions towards the front and rear of the simulation volume. Therefore depending on how the magnetic island overlaps with the ^{13}C seeding plume, material is transported to deposition regions #1 or #2. In the simulation #1 receives more ^{13}C influx & deposition. There is also a deposition region (#3) on the

vertical target but only very little deposition is found on the upper TDU half. There is also very little deposition along the strike line due to strong re-erosion by the plasma due to high T_e in particular towards the rear of the simulation volume.

Computing the line averaged Z_{eff} along the TS-viewline (see Fig. 3) yields $Z_{eff} = 1.264$ which compares well to the experimental values which were in the range from 1.2 to 1.3 with ^{13}C being the dominant contributor. To achieve this value of Z_{eff} the O influx into the plasma was varied (finally a value of $10^{19}(s^{-1})$ was used, see also section 4.1) which affects both the O density but also the C density in the plasma since more O means more C (re-)erosion.

5.1. Comparison to post mortem analysis

After the $^{13}CH_4$ seeding experiment the TDUs were removed and the plasma exposed graphite tiles were analysed by various techniques. In [19] the ^{13}C deposition was measured in each of the 5 TDUs on at the same toroidal location within the TDU on the horizontal target plate in sub-module 2 on finger 6 (TM2h6 see also Figs. 3 and 9). The amount of ^{13}C deposited was measured by elastic backscattering of 2.5 MeV incident protons which yields the areal density of ^{13}C (m^{-2}). In Fig. 10 the ^{13}C deposition along TM2h6 (located in TDU module 30 where ^{13}C was seeded into the plasma) as calculated by WallDYN is compared to the post mortem result. The position values on the x-axis are measured from the edge of the horizontal target that is located at the pumping gap indicated in Fig. 3. Two WallDYN calculations are shown (see also section section 4.1): One with 50% assumed losses to other simulation volumes (WallDYN 50%) and one with no losses (WallDYN 100%). The two results, which can be considered lower and upper bounds for the expected amount of deposited ^{13}C, nicely bound the measured values. It is interesting to note that the reduction in deposition for the 50% WallDYN calculation is different around the strike line (0 to 0.2 (m)) and at the peak deposition region (0.3 to 0.4 (m)) in Fig. 10: At the peak deposition region the deposition is dominated by the influx of ^{13}C directly from the seeding valve which results in a drop in deposition of ≈50% as expected from scaling the redistribution matrix by 50%. In contrast the deposition along the strike line is dominated by deposition from re-erosion sources. These sources are affected by loss of impurities (^{12}C and ^{13}C) from the simulation volume in a non-linear way since they depend on self-sputtering by C-species and multi-step migration.

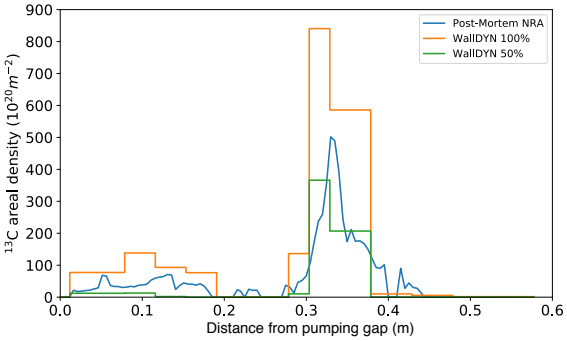

Figure 10: The total deposited amount 10^{20} (m^{-3}) of ^{13}C computed by WallDYN with different assumptions on the loss of ^{13}C to other simulation volumes, compared to the post mortem amount measured along TM2h6.

In Fig. 11 the total ^{13}C erosion erosion rate (1/s) by each projectile species is shown for the final system state after 400 sec of seeded plasma operation (WallDYN 100% case). The total ^{13}C erosion erosion rate is calculated from the erosion flux by each projectile species by multiplying it with the wall element surface area and summing over all wk. The dominant erosion is due to H-ions and H-CX species and self-sputtering (by ^{12}C & ^{13}C) makes up approximately 1/4 of the total erosion rate of ^{13}C. Modelling the self-sputtering of C requires an integrated model of C impurity sources at the wall and re-distribution of C by plasma transport. The erosion rate by O is relatively small due to its very low flux fraction, averaged over the surface of the upper and lower TDU in the simulation: O 0.04% (H + H-CX 98.6%, ^{12}C+^{13}C 1.36%)

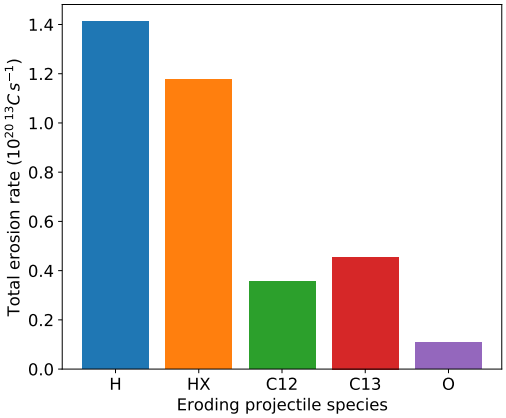

Figure 11: The total ^{13}C erosion erosion rate (1/s) by each projectile species for the final system state after 400 sec of seeded plasma operation

5.2. Importance of impurity recycling in ^{13}C migration modelling

The deposition pattern in Fig. 10 is the result of delicate erosion deposition balance according to eq. 2. In Fig. 12 the contributions to $\frac{\partial \delta_{^{13}C,wk}}{\partial dt}$ are plotted in equilibrium where $\frac{\partial \delta_{^{13}C,wk}}{\partial dt}$ is constant over time and takes on positive values in net deposition- and negative values in net-erosion regions. The total deposited amount shown in Fig. 10 is calculated by integrating $\frac{\partial \delta_{^{13}C,wk}}{\partial dt}$ over time. Since ^{13}C is seeded into the system no net-erosion of ^{13}C

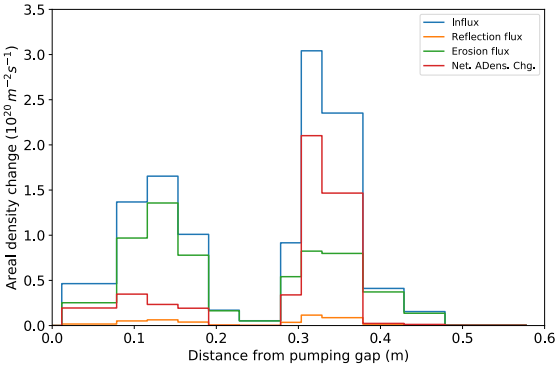

Figure 12: The contributions to flux balance in eq. 2 leading to the local time dependent deposition rate $\frac{\partial \delta_{^{13}C,wk}}{\partial dt}$ (≡Net. ADens. Chg.) along target element. The flux balance for the 100%WallDYN case is shown. (see also Fig. 10)

is possible therefore $\frac{\partial \delta_{^{13}C,wk}}{\partial dt} \geq 0$ everywhere. The region at positions 0.3 to 0.4 (m) from the pumping gap is a clear deposition region where the influx clearly dominates over the erosion and reflection fluxes. However in the deposition region around the strike line (positions 0 to 0.2 (m)) the influx and the erosion flux are very close and the influx wins by a small margin. Clearly small errors in the surface process data (reflection and sputter yields) could tip the balance. For instance just beyond 0.4 m the influx is almost balanced by the re-erosion flux, leading to too low deposition in the calculation compared to the experiment. This shows how important proper modelling of the surface processes is to interpret the experimentally found deposition patterns.

Equally important to the flux balance is the influx of ^{13}C that is computed according to equation 1 based on impurity sources due to seeding, erosion and reflection. While the seeding source is taken directly from the experimental conditions the sources due to erosion and reflection need be calculated self-consistently from solving eqs. 1 and 2 simultaneously. In Fig. 13 the contributions of the three sources: seeding, erosion and reflection to the influx $\Gamma^{In}_{^{13}C,wj,qi}$ at each wall element are shown. According to Fig. 13 the main sources that define incident flux are due to seeding and erosion whereas the relative importance varies. In deposition region 1 & 2 (see Fig. 9) the main contribution is from seeding whereas deposition around the strikeline is dominated by (re-)erosion. For the deposition region 3 on the vertical target the contribution of seeding and (re-)erosion is similar. Since for C on C the reflected flux is quite low, even at 40° impact angle, the contribution of the reflected source is low. This however is different when the mass ratio of incident species to surface species (e.g. Be on W in ITER) is $\ll 1$, then the reflection yield is high and so is its contribution to the incident flux. The importance of the re-erosion flux again shows the importance if integrated modelling of surface processes and plasma transport.

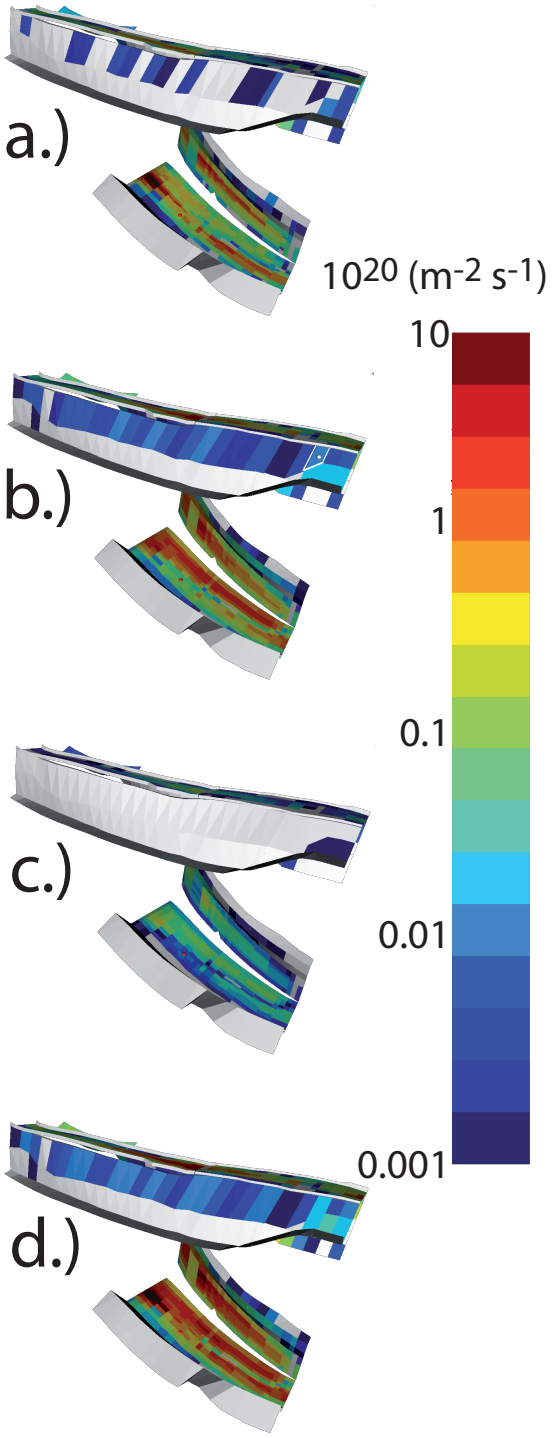

Figure 13: Comparison of the contribution of different sources to the influx of ^{13}C onto each wall element: a.) Seeding, b.) (re-)erosion c.) reflection d.) Sum of all contributions i.e. the total ^{13}C influx.

6. Conclusions

The newly developed [12, 13] 3D version of WallDYN was used to model the $^{13}CH_4$ seeding experiment in W7-X. Using a background plasma solution that reasonably matches the plasma conditions during the 30 seeded discharges, the redistribution matrix for C isotopes was computed. Using this redistribution matrix together with erosion yield data from literature and SDTrim.SP the coupled evolution of surface composition and impurity influx from the plasma was calculated using the WallDYN approach. A comparison with first available post mortem data shows good agreement with the modelling results. Investigating the different contributions to layer deposition and incident fluxes shows the importance of impurity recycling and the need for integrated modelling of surface dynamics and plasma transport.

7. Acknowledgment

This work has been carried out within the framework of the EUROfusion Consortium and has received funding from the Euratom research and training programme 2014-2018 and 2019-2020 under grant agreement No 633053. The views and opinions expressed herein do not necessarily reflect those of the European Commission.

[1] A. Hakola, M. I. Airila, C. Björkas, D. Borodin, S.Brezinsek, J. P. Coad, M. Groth, A. Järvinen, A. Kirschner, S. Koivuranta, T. K.-S. K. Krieger, J. Likonen, V. Lindholm, T. Makkonen, J. M. M. Mayer, H. W. Müller, R. Neu, P. Petersson, V. Rohde, M. Rubel, A. Widdowson, the ASDEX Upgrade Team, J.-E. Contributors, Global migration of impurities in tokamaks, Plasma Phys. Control. Fusion 55 (2013) 124029.

[2] R. Schneider, X. Bonnin, K. Borrass, D. Coster, Contrib. Plasma Phys. 46 (2006) 3.

[3] Y. Feng, F. Sardei, J. Kisslinger, P. Grigull, K. McCormick, D. Reiter, Contrib. Plasma Phys. 1-3 (2004) 57.

[4] P. Stangeby, J. D. Elder, J. Nucl. Mater. 196-198 (1992) 258.

[5] A. Kirschner, V. Philipps, J. Winter, U. Kögler, Nucl. Fusion 40 (2000) 989.

[6] A. Mutzke, R. Schneider, W. Eckstein, R. Dohmen IPP-Report 12/8.

[7] W. Möller, W. E. und J. P. Biersack, Computer Physics Communications 51 No. 8 (1988) 355.

[8] K. Schmid, M. Reinelt, K. Krieger, J. Nucl. Mater. 415 (2011) 284.

[9] K. Schmid, K. Krieger, S. W. Lisgo, G. Meisl, S. Brezinsek, J. E. Contributors, J. Nucl. Mater. 463 (2015) 66.

[10] V.Philipps, Ph.Mertens, G.F.Matthews, H.Maier, J.-E. contributors, Fusion Engineering and Design 7-9 (2010) 1581.

[11] G. Meisl, K. Schmid, M. Oberkofler, K. Krieger, S. Lisgo, L. Aho-Mantila, F. Reimold, A. U. Team, Nitrogen retention in asdex upgrade, Journal of Nuclear Materials 463 (2015) 668.

[12] K. Schmid, T. Lunt, 3d global impurity transport modeling with walldyn and emc3-eirene, Nuclear Materials and Energy 17 (2018) 200.

[13] K. Schmid, T. Lunt, Physica Scripta T171 (2020) 014006.

[14] M. Reinelt, K. Krieger, S. Lisgo, K. Schmid, S. Brezinsek, J. E. Contributors, Interpretation of be migration studies at jet and validation of an integrated numerical model for plasma impurity transport and wall composition dynamics, Journal of Nuclear Materials 415 (2011) S305.

[15] K. Schmid, M. J. Baldwin, R. P. Doerner, D. Nishijima, Be layer deposition on carbon and tungsten from beryllium seeded plasmas, Nuclear Technology 159 (2007) 238.

[16] K. Schmid, J. Roth, Erosion of high-z metals with typical impurity ions, Journal of Nuclear Materials 313 (2003) 302.

[17] M. Küstner, W. Eckstein, E. Hechtl, J. Roth, Angular dependence of the sputtering yield of rough beryllium surfaces, Journal of Nuclear Materials 265 (1999) 22.

[18] T. S. Pedersen, R. König, M. Krychowiak, M. Jakubowski, J. Baldzuhn, S. Bozhenkov, G. Fuchert, A. Langenberg, H. Niemann, D. Zhang, K. Rahbarnia, H. S. Bosch, Y. Kazakov, S. Brezinsek, Y. Gao, N. Pablant, the W7-X Team, First results from divertor operation in wendelstein 7-x, Plasma Phys. Control. Fusion 61 (2019) 014035.

[19] M. Mayer, Material erosion, deposition and transport in the divertor region of the stellarator w7-x, These proceedings.

[20] Y. Feng, H. Frerichs, M. Kobayashi, A. Bader, F. Effenberg, D. Harting, H. Hoelbe, J. Huang, G. Kawamura, J. D. Lore, T. Lunt, D. Reiter, O. Schmitz, , D. Sharma, Recent improvements in the emc3-eirene code, Contrib. Plasma Phys. 54 (4-6) (2014) 426.

[21] F. Effenberg, H. Niemann, Y. Feng, J. Geiger, O. Schmitz, Y. Suzuki, A. Ali, T. Barbui, S. Brezinsek, H. Frerichs, M. Jakubowski, R. König, M. Krychowiak, A. P. Sitjes, J. Schmitt, T. S. Pedersen, W.-X. Team, Investigation of 3d effects on heat fluxes in performance-optimized island divertor configurations at wendelstein 7-x, Nuclear Materials and Energy 18 (2019) 262.

[22] R. Laube, M. Laux, M. Y. Yea, H. Greuner, S. Lindig, Designs of langmuir probes for w7-x, Fusion Engineering and Design 86 (2011) 1133.

[23] E. Pasch, M. N. A. Beurskens, S. A. Bozhenkov, G. Fuchert, J. Knauer, R. C. Wolf, , W.-X. T. E. Pasch, M. N. A. Beurskens, S. A. Bozhenkov, G. Fuchert, J. Knauer, R. C. Wolf, , W.-X. Team, The thomson scattering system at wendelstein 7-x, Rev. Sci. Instrum. 87 (2016) 11E729.

[24] P. C. Stangeby, The plasma boundary of magnetic fusion devices, IOP Pulishing, 2000.

[25] J. Roth, C. García-Rosales, Nucl. Fusion 37 (1997) 897.

[26] E. Hechtl, J. Bohdansky, Carbon monoxide formation on graphite bombarded with oxygen ions, J. Nucl. Mater. 154 (1988) 201.

[27] E. Hechtl, J. Bohdansky, Sputtering of pyrolytic graphite with oxygen ions at various target temperatures, Journal of Nuclear Materials 141-143 (1986) 139.

[28] K. Schmid, M. Mayer, C. Adelhelm, M. Balden, S. L. et al, Nucl. Fusion 50 (2010) 105004.